Energy 192 (2020) 116631

Contents lists available at ScienceDirect

Energy

journal homepage: www.elsevier.com/locate/energy

Coordinated allocation of distributed generation resources and electric vehicle charging stations in distribution systems with vehicle-to-grid interaction

Lizi Luo [a], Zhi Wu [b, c, *], Wei Gu [c], He Huang [d], Song Gao [d], Jun Han [e]

[a] School of Automation, Nanjing University of Science and Technology, Nanjing, 210094, China
[b] Jiangsu Key Laboratory of Smart Grid Technology and Equipment, Nanjing, 210096, China
[c] School of Electrical Engineering, Southeast University, Nanjing, 210096, China
[d] State Grid Jiangsu Electric Power CO., LTD., Nanjing, 210024, China
[e] State Grid Jiangsu Economic Research Institute, Nanjing, 210008, China

ARTICLE INFO

Article history:
Received 11 November 2018
Received in revised form
15 November 2019
Accepted 25 November 2019
Available online 29 November 2019

Keywords:
Coordinated allocation
Distributed generation resource (DGR)
Distribution system
Electric vehicle charging station (EVCS)
Mixed integer second order cone programming (MISOCP)
Vehicle-to-grid (V2G)

ABSTRACT

With the implementation of vehicle-to-grid technologies, electric vehicles in distribution systems are becoming controllable resources and enabled to provide a lot of ancillary services (e.g. peak power shaving, voltage regulation, spinning reserve and so on). This phenomenon brings positive effects to the operation of distribution systems but simultaneously challenges the deployments of related power devices, especially the distributed generation resources. Based on this background, this paper proposes an optimization model to jointly deploy electric vehicle charging stations and distributed generation resources, during which the vehicle-to-grid function of electric vehicles is comprehensively considered. To make the optimization model ideally convex, linearized Distflow equations, as well as an exact second order conic relaxation are adopted and utilized in this paper. Consequently, the proposed model can be efficiently solved by off-the-shelf commercial solvers and the allocation schemes with minimal annualized social costs are obtained in polynomial time. Finally, a practical urban area fed by a 31-bus distribution system in China is selected as the test system to verify the effectiveness of the proposed approach, and numerical results are analyzed.

1. Introduction

With the growing concern on fossil fuel exhaustion and worldwide climate change, the integration of renewable energy resources and electric vehicles (EVs) in distribution systems has attracted wide attention in the past decade [1]. EVs with vehicle-to-grid (V2G) functions can be regarded as ideally controllable resources that provide ancillary services to distribution systems, such as peak power shaving, voltage regulation and stability enhancement [2]. These ancillary services effectively relieve the negative effects caused by the intermittency of renewable energy, and in consequence make the distribution system operate in a cost-effective way [3]. Therefore, as typical integration modes of renewable energy resources and EVs, the coordinated allocation of distributed generation resources (DGRs) and electric vehicle charging stations (EVCSs) under V2G environment deserves intensive researches and would bring about significant benefits.

The optimal allocation of DGRs and EVCSs, as well as V2G technologies of EVs has become research hotspot in recent years. The relevant literatures are reviewed respectively as follows.

With regard to the optimal allocation of DGRs and EVCSs, researches have been carried out from diverse perspectives and referred to various application scenarios. In Ref. [4], DGRs including wind turbines, photovoltaic modules, diesel generators and energy storage systems are jointly planned for the purpose of minimizing annual distribution system operation cost. In Ref. [5], an electric power system reliability check is properly involved in the optimal allocation of EVCSs, and thereby constraints derived from power system operation as well as EV owners' requirements are comprehensively considered. In Ref. [6], a two-stage approach is

* Corresponding author. Jiangsu Key Laboratory of Smart Grid Technology and Equipment, Nanjing, 210096, China.
E-mail addresses: luolizi@126.com (L. Luo), zwu@seu.edu.cn (Z. Wu), wgu@seu.edu.cn (W. Gu), huh@js.sgcc.com.cn (H. Huang), 13913047929@139.com (S. Gao), hjchallenge@126.com (J. Han).

https://doi.org/10.1016/j.energy.2019.116631
0360-5442/

Nomenclature

Indices

k	EV index
n	Land block index
t	Time segment index
s	Season index
i/j	Electrical bus index

Sets

$u(i)/u(j)$	Downstream buses connected to bus i/j
$v(j)$	Upstream buses connected to bus j
$\Omega_{d/nd}$	Dispatchable/non-dispatchable EVs
Ω_S	Substation buses in the distribution system
Ω_N	Electrical buses in the distribution system
Ω_L	Branches in the distribution system
$\Omega_{PV/MT/CF}$	Candidate buses of PV/MT/EVCS
Ω_j^{bus}	Electrical buses included in the service region of EVCS installed at bus j
$\Omega_{s,i,t}^{EV}$	EVs whose parking durations cover time segment t and are heading for bus i in season s

Parameters

ir_{rated}	PV rated solar irradiance (W/m^2)
$P_{ir\text{-}rated}$	PV active power output under ir_{rated} (kW)
$S_{PV\text{-}rated}$	PV rated capacity (kVA)
$S_{MT\text{-}rated}$	MT rated capacity (kVA)
EV_k	Electric vehicle numbered k
P_{EV}^{rated}	EV rated charging power (kW)
T_k^{park}	Parking duration of EV_k (time segment)
Δt	Span of each time segment (i.e. 15 min in this paper)
$Cap_{k/(s,i,k)}$	Rated battery capacity of $EV_k/EV_{s,i,k}$ (kWh)
SOC_k	State of charge of EV_k
N_n	Total number of EVs heading for land block n
N_b	Total number of land blocks in the target area
N_{bus}	Total number of electrical buses in the system
$c_{PV/MT/CF}^{I}$	Per-unit investment cost of PV/MT/CF ($)
d	Discount rate
$y_{PV/MT/CF}$	Economic life of PV/MT/CF (year)
$c_{PV/MT/CF}^{O\&M}$	Per unit O&M cost of PV/MT/CF ($)
c_{MT}^{F}	Per-unit fuel cost of MT power generation ($/kWh)
c_{em}^{C}	Per-unit tax cost of CO_2 emission ($/g)
ρ_{em}	CO_2 emission of per-unit MT power generation (g/kWh)
c^P	Per-unit cost of purchasing electricity from upper grid ($/kWh)
c^{NL}	Per-unit cost of network losses ($/kWh)
R_{ij}/X_{ij}	Resistance/reactance of branch from i to j (Ω)
c^{CL}	Per-unit cost of electricity losses in charging/discharging ($/kWh)
η	Power loss rate in charging/discharging
c^B	Per-unit cost of EV battery degradation ($/kWh)
U_{sub}	Voltage magnitude of substation bus (kV)
$U_{\min}/U_{\max}$	Lower/upper limit of voltage magnitude (kV)
$I_{ij,max}$	Permitted maximum current in branch ij (A)
$S_{PV/MT}^{unit}$	Available unit capacity of PV/MT (kVA)
$Q_{PV,lim}^{unit}$	Maximum limit for the reactive power output of each PV unit (kVar)
b	Upper bound of integer variable $B_{s,i,k,t}^{dis}$
$EV_{s,i,k}$	kth EV among EVs heading for bus i in season s
$T_{i,k}^{ar}$	Arriving time of $EV_{s,i,k}$ (time segment)
$T_{i,k}^{park}$	Parking duration of $EV_{s,i,k}$ (time segment)
r	Growth rate of investment and O&M cost in modifying unidirectional CFs into bidirectional CFs

Variables

ir	Solar irradiance (W/m^2)
P_{ir}/Q_{ir}	PV active/reactive power output under ir (kW/kVar)
P_{MT}	MT active power output (kW)
$E_{k/(s,i,k)}$	Rechargeable battery capacity of $EV_k/EV_{s,i,k}$
C^I	Annualized investment cost ($)
$C^{O\&M}$	Annual cost of O&M ($)
$C^{F\&E}$	Annual cost of fuel and carbon emission ($)
C^P	Annual cost of purchasing electricity from upper grid ($)
C^{NL}	Annual cost of network losses ($)
C^{CL}	Annual cost of electricity losses in charging/discharging ($)
C^B	Annual cost of EV battery degradation ($)
$R_{PV/MT/CF}$	Investment recovery factors for PV/MT/CF
$S_{PV,i}^{rated}/S_{MT,i}^{rated}$	Rated capacity of PV/MT at bus i (kVA)
$N_i^{PV/MT/CF}$	Integer variable that reveals the installation number of PV/MT/CF at bus i
$P_{PV/MT,s,t,i}^{WO/WD}$	PV/MT active power output at bus i under time segment t in the typical workday/weekend of season s (kW)
$P_{s,t,ij}^{WO/WD}$	Power flow in branch ij at time segment t in the typical workday/weekend of season s (kW)
$I_{s,t,ij}^{sqr,WO/WD}$	Square of current in branch ij at time segment t in the typical workday/weekend of season s
$N_{CF,s,t,i}^{WO/WD}$	Quantities of occupied (in-use) CFs at bus i under time segment t in the typical workday/weekend of season s
$P_{s,t,ij}/Q_{s,t,ij}$	Active/reactive power flow in branch ij at time segment t in season s (kW/kVar)
$P_{s,t,j}^{eq}/Q_{s,t,j}^{eq}$	Equivalent active/reactive power demand at bus j under time segment t in season s (kW/kVar)
$U_{s,t,i}$	Voltage magnitude at bus i corresponding to time segment t in season s (kV)
$P_{s,t,j}^{Load}/Q_{s,t,j}^{Load}$	Active/reactive load demand at bus j under time segment t in season s (kW/kVar)
$P_{s,t,j}^{PV/MT}$	Unified representation of *PWO/WD PV,s,t,j/PWO/WD MT,s,t,j*
$P_{s,t,j}^{EV}$	Power demand of EVCS at bus j under time segment t in season s (kW)
$Q_{s,t,j}^{PV}$	PV reactive power output at bus j under time segment t in season s (kVar)
$B_{s,i,k,t}^{cha/dis}$	Binary variable indicates charging/discharging state of $EV_{s,i,k}$ at time segment t
Au	Auxiliary variable in relaxation
$\Delta_{s,t,ij}$	Deviation variable employed to verify the exactness of second order conic relaxation

proposed for the coordinated allocation of DGRs and EVCSs in distribution systems, during which the economic benefits of EV parking lot investors and the technical constraints of distribution system operators (DSOs) are fully concerned. To overcome the complexity of allocation model, second order conic relaxation is applied to the branch power flow constraints in Ref. [7] and thereby the allocation model of PV power generation and EVCSs is formulated as a second order cone programming (SOCP) model, which is ideally convex and can be efficiently solved by off-the-shelf commercial solvers. Furthermore, an accelerated Generalized Benders Decomposition algorithm is employed in Ref. [8] to expedite the large computation caused by numerous operation scenarios. In Ref. [9], a Markov Chain Monte Carlo (MCMC) simulation model is utilized to account for the uncertainties of EV charging demands and renewable power generation. Subsequently the coordinated control of EV charging demands, DGR outputs, and energy storage charging/discharging behaviors are incorporated in the allocation model.

Similarly, in terms of the V2G technologies of EVs, relevant researches can be found in numerous literatures. In Refs. [10,11], concepts of unidirectional and bidirectional V2G are systematically expounded, respectively. Under unidirectional V2G environment, charging power rates and charging time intervals of EVs are adjustable to provide ancillary services. While for bidirectional V2G, the power flow reversal is allowed and thereby the impacts of EVs in distribution systems are accordingly strengthened, especially on power demand curve, frequency control and risk management [12]. In Ref. [13], a scenario of V2G implementation within regional power grids is discussed, and the overall load variance is minimized on the basis of a double-layer optimal charging strategy. In Ref. [14], an optimal scheduling algorithm for EVs with V2G functions is formulated, through which the financial benefits of customers and aggregators are simultaneously considered. In Ref. [15], a novel agent-based coordinated dispatch strategy for EVs and DGRs is proposed, and thereby make EVs and DGRs accommodate practical implementation in a more efficient way. In Ref. [16], a pricing policy is designed for liberating V2G price from the market electricity price, based on which EV owners are motivated to participate in V2G activities and meanwhile aggregators' profits are ensured. Furthermore, combined biddings of ancillary services for EVs with V2G functions are intensively researched in Ref. [17], which make the market environment more comprehensive.

From the literature review above, it is obvious that most of the existing researches concerning EVs' V2G technologies are focused on operation problems (e.g. economic and security influence analysis, optimization on charging strategy, market establishment for ancillary service). Very few researches take account of EVs' V2G interaction with distribution systems in the planning stage, especially in the coordinated allocation of DGRs and EVCSs. However, the ancillary services provided by EVs with V2G functions distinctly impact the temporal distribution of EV charging power, and in consequence bring about numerous positive effects to the integration of DGRs. Taking EVs' V2G functions into consideration during the deployment of DGRs and EVCSs accords with the future application scenarios in smart distribution systems, and has the potential to generate distinct economic benefits.

Based on this background, this paper proposes a comprehensive model to jointly deploy EVCSs and DGRs, during which the V2G function of EVs is fully considered. With photovoltaic (PV) power generation and gas-based micro-turbines (MTs) selected as the typical representatives of DGRs, the optimal sites and sizes of DGRs, as well as the optimal sizes of EVCSs are determined with the target of minimizing annualized social costs. The main contributions of this paper are summarized as follows.

1) V2G functions of EVs are properly considered in the proposed optimization model. To be specific, EV charging demands are regarded as controllable resources, and the optimal scheduling problem of EVs is embedded into the allocation problem.
2) The concept of PV-STATCOM that utilizes the unused capacity of PV inverter as STATCOM is considered in this paper. And the reactive power output of PV power generation is regarded to be adjustable according to the operation state of distribution system.
3) Accompanied with the linearized Distflow equations, an exact second order conic relaxation is proposed and adopted, which makes the optimization model formulated as a mixed integer second order cone programming (MISOCP) problem.
4) The proposed research is based on coupled geographical-electrical systems, and a practical urban area in China is selected as the test system.

The remaining parts of this paper are organized as follows. Section 2 explains the modeling methods of DGR outputs, EV charging demands and electrical loads. Section 3 minutely describes the proposed allocation model, as well as the exact second order conic relaxation. Numerical results are presented and analyzed in Section 4. And finally, conclusion is summarized in Section 5.

2. Modeling of relevant resources and loads

This section explains the representation of DGR outputs, EV charging demands and electrical loads, which is the basis of the coordinated allocation problem.

2.1. Assumption and discretization

To relieve the complexity of the proposed allocation problem, and meanwhile reduce the computation burden in the solving process, the continuous time horizons concerned in this paper are properly discretized. The specific simplification and assumption are shown as follows.

1) Eight typical days are generated to represent a certain year. These typical days correspond to workdays and weekends in Spring, Summer, Autumn, Winter, respectively.
2) Each typical day is further subdivided into 96 time segments (15 min each).
3) Variations of DGR outputs, EV charging power, electrical loads within a time segment are neglected. That is to say, each time segment is simplified as a deterministic scenario.

2.2. Modeling of distributed generation resource outputs

For PV power generation, solar irradiance is usually thought to be the dominant factor that affects their active power outputs. As a simple and effective method to represent the temporal variation of solar irradiance in certain areas, the typical distribution curves of solar irradiance are fitted through historical data in this paper. For the direct perception of readers, Fig. 1 shows a group of typical distribution curves of solar irradiance, which are derived from the public data measured in Moab, Utah, USA [18]. Seasonality has been fully considered in the fitting process, as marked by different colors in Fig. 1. And meanwhile, for the purpose of concision, solar irradiance is shown in per unit value, whose base value is set to be the annual peak solar irradiance.

Given solar irradiance, PV active power outputs can be calculated through a simplified piecewise function [19], as shown in (1).

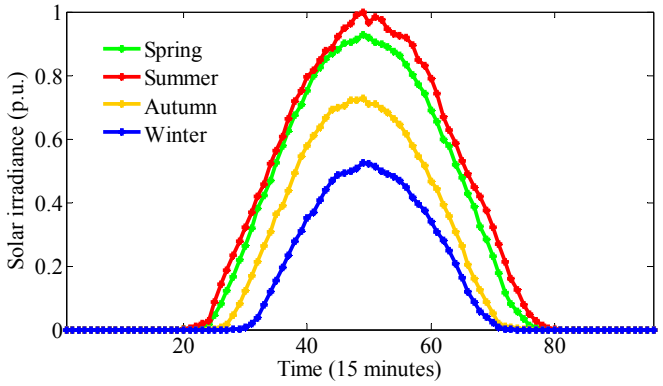

Fig. 1. A group of typical distribution curves of solar irradiance.

And moreover, with the concept of PV-STATCOM developed in recent years [20], the unused capacities of PV inverters are utilized to provide reactive power in this paper, which brings significant benefits to the operation of distribution system. The reactive power outputs of PV power generation are ideally controllable, and their adjustable ranges are formulated in (2) [21].

$$P_{ir}=\begin{cases} P_{ir-rated}\cdot\dfrac{ir}{ir_{rated}}, & 0\le ir\le ir_{rated} \\ P_{ir-rated}, & ir_{rated}<ir \end{cases} \tag{1}$$

$$-\sqrt{S_{PV-rated}^2-P_{ir}^2}\le Q_{ir}\le\sqrt{S_{PV-rated}^2-P_{ir}^2} \tag{2}$$

While for gas-based MTs, they are regarded as pure active power sources in this paper from the economic perspective, and their actual outputs are determined by the optimal scheduling schemes of distribution systems. With regard to a particular gas-based MT, the adjustable range of active power output is shown as follows.

$$0\le P_{MT}\le S_{MT-rated} \tag{3}$$

2.3. Modeling of electric vehicle charging demands

This paper concentrates on the charging behaviors of private EVs in urban areas, and the "destination charging" [22] mode is assumed to be adopted by EV owners. In consequence, parking behaviors of EV owners are the key factors that determine EV charging behaviors in this paper. Details of the "destination charging" mode, as well as the representation of EV parking behaviors have been systematically expounded in Ref. [22], and readers may refer to this literature for more information. Moreover, for readers' convenience, a group of typical distribution curves of EVs' arrival numbers and parking durations collected from Ref. [22] are attached in Appendix A.

On the other aspect, state of charge (SOC) reflects the statue of EV battery and is an important factor that should be carefully considered in the modeling EV charging demands. In this paper, SOCs of the arriving EVs are assumed to be uniformly distributed in the interval [0, 1], and the SOC of each EV is randomly generated. Subsequently, the arriving EVs can be divided into two types (i.e. dispatchable ones and non-dispatchable ones), as shown in (4).

$$\begin{cases} EV_k\in\Omega_d & if\ \ E_k\Big/P_{EV}^{rated}<T_k^{park}\cdot\Delta t \\ EV_k\in\Omega_{nd} & if\ \ E_k\Big/P_{EV}^{rated}\ge T_k^{park}\cdot\Delta t \end{cases} \tag{4}$$

where

$$E_k=Cap_k\cdot(1-SOC_k) \tag{5}$$

It is obvious that EVs can be dispatched only when they have long enough park durations to make their batteries fully charged. While for those EVs that are impossible to be fully charged due to short park duration, they should be charged at rated power as soon as they enter the parking lots, until departures. Charging schemes of those EVs are fixed and in consequence they are classified as non-dispatchable EVs in (4).

Finally, based on the acquired distribution curves of EVs' arrival numbers and parking durations, as well as SOCs, the representation of EV charging demands for each typical day can be properly generated. The flowchart is shown in Fig. 2.

2.4. Modeling of electrical loads

The modeling method of electrical loads utilized in this paper has been minutely described in Ref. [22], where readers can find very detailed information. And moreover, for the direct perception of readers, a group of typical load profiles collected from Ref. [22] is provided in Appendix B.

3. Optimization model

This section describes the proposed optimization model, as well as its exact relaxation for the coordinated allocation of DGRs and EVCSs.

3.1. Objective function

Benefits of diverse interest subjects have been comprehensively considered in this paper, from the perspective of a social planner. To be specific, the annualized social cost related with DGRs and EVCSs is set to be the objective function of allocation model, whose expression is shown in (6).

$$\min\quad Cost=C^I+C^{O\&M}+C^{F\&E}+C^P+C^{NL}+C^{CL}+C^B \tag{6}$$

where C^I, $C^{O\&M}$, $C^{F\&E}$, C^P, C^{NL}, C^{CL} and C^B stand for the annualized investment cost, annual cost of operation and maintenance (O&M), annual cost of fuel and carbon emission, annual cost of purchasing electricity from upper grid, annual cost of network losses, annual cost of electricity losses in charging/discharging behaviors, and annual cost of EV battery degradation, respectively. As a reasonable simplification, each season is assumed to be composed of 65.25 workdays and 26 weekends in this paper. Then the specific representation of each cost item is provided in (7)–(16).

3.1.1. Annualized investment cost

$$C^I=R_{PV}\cdot\sum_{i=1}^{N_{bus}}\left(c_{PV}^I\cdot S_{PV,i}^{rated}\right)+R_{MT}\cdot\sum_{i=1}^{N_{bus}}\left(c_{MT}^I\cdot S_{MT,i}^{rated}\right)+R_{CF}\cdot\sum_{i=1}^{N_{bus}}\left(c_{CF}^I\cdot N_i^{CF}\right) \tag{7}$$

where R_{PV}, R_{MT} and R_{CF} are respectively investment recovery factors

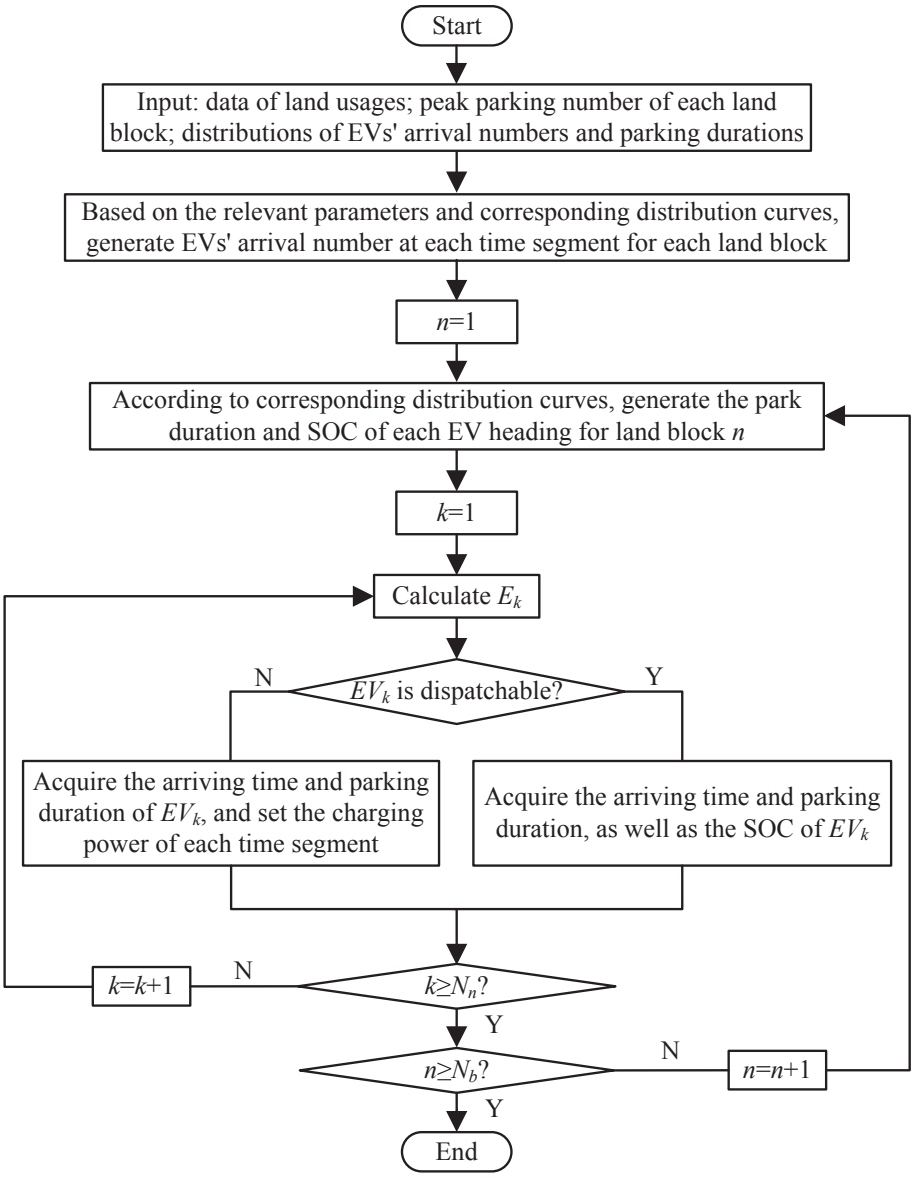

Fig. 2. Flowchart for the representation of EV charging demands.

corresponding to PV power generation, MTs and EV charging facilities (CFs). These factors are ratios used to calculate the present value of an annuity (a series of equal annual cash flows) [23].

$$R_{PV} = \frac{d(1+d)^{y_{PV}}}{(1+d)^{y_{PV}} - 1} \tag{8}$$

$$R_{MT} = \frac{d(1+d)^{y_{MT}}}{(1+d)^{y_{MT}} - 1} \tag{9}$$

$$R_{CF} = \frac{d(1+d)^{y_{CF}}}{(1+d)^{y_{CF}} - 1} \tag{10}$$

3.1.2. Annual cost of O&M

$$\begin{aligned} C^{O\&M} = 65.25 \cdot \sum_{s=1}^{4}\sum_{t=1}^{96}\sum_{i=1}^{N_{bus}}\left[\left(c_{PV}^{O\&M}\cdot P_{PV,s,t,i}^{WO} + c_{MT}^{O\&M}\cdot P_{MT,s,t,i}^{WO}\right)\cdot \Delta t\right] \\ +26 \cdot \sum_{s=1}^{4}\sum_{t=1}^{96}\sum_{i=1}^{N_{bus}}\left[\left(c_{PV}^{O\&M}\cdot P_{PV,s,t,i}^{WD} + c_{MT}^{O\&M}\cdot P_{MT,s,t,i}^{WD}\right)\cdot \Delta t\right] \\ +\sum_{i=1}^{N_{bus}}\left(c_{CF}^{O\&M}\cdot N_i^{CF}\right) \end{aligned} \tag{11}$$

This item consists of the annual O&M costs of PV power generation, MTs and CFs. The DGRs' annual O&M costs are correlated with their actual active power outputs. While for CFs, the annual O&M cost of each CF is a constant parameter.

3.1.3. Annual cost of fuel and carbon emission

$$C^{F\&E} = 65.25 \cdot \left(c^{F}_{MT} + c^{C}_{em} \cdot \rho_{em}\right) \cdot \sum_{s=1}^{4} \sum_{t=1}^{96} \sum_{i=1}^{N_{bus}} \left[P^{WO}_{MT,s,t,i} \cdot \Delta t\right] + 26 \cdot \left(c^{F}_{MT} + c^{C}_{em} \cdot \rho_{em}\right) \cdot \sum_{s=1}^{4} \sum_{t=1}^{96} \sum_{i=1}^{N_{bus}} \left[P^{WD}_{MT,s,t,i} \cdot \Delta t\right] \tag{12}$$

As fossil fuel-based DGRs, MTs are involved into the calculation of annual fuel and carbon emission costs. The numerical value of this cost item is directly determined by actual active power outputs of MTs.

3.1.4. Annual cost of purchasing electricity from upper grid

$$C^{P} = 65.25 \cdot \sum_{s=1}^{4} \sum_{t=1}^{96} \sum_{i \in \Omega_S} \sum_{j \in u(i)} \left[c^{P} \cdot P^{WO}_{s,t,ij} \cdot \Delta t\right] + 26 \cdot \sum_{s=1}^{4} \sum_{t=1}^{96} \sum_{i \in \Omega_S} \sum_{j \in u(i)} \left[c^{P} \cdot P^{WD}_{s,t,ij} \cdot \Delta t\right] \tag{13}$$

Besides of the power generated by DGRs, DSOs have to purchase electricity from upper grid to maintain the operation of distribution systems. This part of annual cost can be derived from the active power injection via feeders connected with substation.

3.1.5. Annual cost of network losses

$$C^{NL} = 65.25 \cdot \sum_{s=1}^{4} \sum_{t=1}^{96} \sum_{i=1}^{N_{bus}} \sum_{j \in u(i)} \left[c^{NL} \cdot I^{sqr,WO}_{s,t,ij} \cdot R_{ij} \cdot \Delta t\right] + 26 \cdot \sum_{s=1}^{4} \sum_{t=1}^{96} \sum_{i=1}^{N_{bus}} \sum_{j \in u(i)} \left[c^{NL} \cdot I^{sqr,WD}_{s,t,ij} \cdot R_{ij} \cdot \Delta t\right] \tag{14}$$

Since the power flow equations employed in this paper have neglected network losses, as detailedly illustrated in the next subsection, the annual network losses cost is excluded in (13) and should be calculated individually.

3.1.6. Annual cost of electricity losses in charging/discharging behaviors

$$C^{CL} = 65.25 \cdot \sum_{s=1}^{4} \sum_{t=1}^{96} \sum_{i=1}^{N_{bus}} \left[c^{CL} \cdot \eta \cdot P^{rated}_{EV} \cdot N^{WO}_{CF,s,t,i} \cdot \Delta t\right] + 26 \cdot \sum_{s=1}^{4} \sum_{t=1}^{96} \sum_{i=1}^{N_{bus}} \left[c^{CL} \cdot \eta \cdot P^{rated}_{EV} \cdot N^{WD}_{CF,s,t,i} \cdot \Delta t\right] \tag{15}$$

Electricity losses are inevitable in EV charging/discharging behaviors, and should be properly included in the calculation of annual cost. For the purpose of simplification, the adjustable characteristic of EVs' charging power is neglected in this paper. That is to say, EV charging facilities under charging and discharging scenarios can only operate at rated power.

3.1.7. Annual cost of EV battery degradation

$$C^{B} = 65.25 \cdot \sum_{s=1}^{4} \sum_{t=1}^{96} \sum_{i=1}^{N_{bus}} \left[c^{B} \cdot P^{rated}_{EV} \cdot N^{WO}_{CF,s,t,i} \cdot \Delta t\right] + 26 \cdot \sum_{s=1}^{4} \sum_{t=1}^{96} \sum_{i=1}^{N_{bus}} \left[c^{B} \cdot P^{rated}_{EV} \cdot N^{WD}_{CF,s,t,i} \cdot \Delta t\right] \tag{16}$$

As an important part of objective function, the cost of EV battery degradation is derived from the charging/discharging behaviors supporting EVs' daily driving and V2G participation, and directly reflects the economic life reduction of EV batteries. In this paper, the correlation between EV battery degradation cost and EV charging/discharging electricity is simplified as a linear one [24].

3.2. Constraints

This subsection describes the constraints employed in the proposed coordinated allocation model. For the purpose of concision, constraints corresponding to workdays and weekends are represented in a unified way when confusion unlikely occurs.

3.2.1. Power flow equations

$$\sum_{i \in v(j)} P_{s,t,ij} = \sum_{l \in u(j)} P_{s,t,jl} + P^{eq}_{s,t,j} \quad \forall s,t, \quad \forall j \in \Omega_N \tag{17}$$

$$\sum_{i \in v(j)} Q_{s,t,ij} = \sum_{l \in u(j)} Q_{s,t,jl} + Q^{eq}_{s,t,j} \quad \forall s,t, \quad \forall j \in \Omega_N \tag{18}$$

$$U_{s,t,j} = U_{s,t,i} - \frac{P_{s,t,ij} \cdot R_{ij} + Q_{s,t,ij} \cdot X_{ij}}{U_{sub}} \quad \forall s,t, \quad \forall ij \in \Omega_L \tag{19}$$

where U_{sub} corresponds to the voltage magnitude of substation bus and is valued 1 p.u. in this paper. Equations 17–19 are the linearized Distflow equations, which have been extensively used and justified in numerous studies concerning optimization problems of distribution systems [25].

3.2.2. Equivalent load demands at buses

$$P^{eq}_{s,t,j} = P^{Load}_{s,t,j} - P^{PV}_{s,t,j} - P^{MT}_{s,t,j} + P^{EV}_{s,t,j} \quad \forall s,t, \quad \forall j \in \Omega_N \tag{20}$$

$$Q^{eq}_{s,t,j} = Q^{Load}_{s,t,j} - Q^{PV}_{s,t,j} \quad \forall s,t, \quad \forall j \in \Omega_N \tag{21}$$

With consideration of the power generation and consumption from diverse devices, the equivalent load demand at each bus is calculated through (20) and (21).

3.2.3. Restrictions on voltage magnitudes

$$U_{min} \le U_{s,t,i} \le U_{max} \quad \forall s,t, \quad \forall i \in \Omega_N \tag{22}$$

As common restrictions on the operation of distribution systems, voltage magnitudes of all the electrical buses must be kept within ranges defined by lower and upper limits.

3.2.4. Restrictions on branch current

$$I_{s,t,ij}^{sqr}=\frac{P_{s,t,ij}^2+Q_{s,t,ij}^2}{U_{sub}^2} \quad \forall s,t, \quad \forall ij\in\Omega_L \tag{23}$$

$$I_{s,t,ij}^{sqr}\le I_{ij,max}^2 \quad \forall s,t, \quad \forall ij\in\Omega_L \tag{24}$$

Like the simplification in linearized Distflow equations, a simplified branch current expression [26] is employed in this paper, as shown in (23). For each branch, there exists a permitted maximum branch current.

3.2.5. Discrete size constraints for DGRs

$$S_{PV,i}^{rated}=N_i^{PV}\cdot S_{PV}^{unit} \quad \forall i\in\Omega_{PV} \tag{25}$$

$$S_{MT,i}^{rated}=N_i^{MT}\cdot S_{MT}^{unit} \quad \forall i\in\Omega_{MT} \tag{26}$$

Since DGRs are commercially available in discrete sizes, the installed PV and MT capacities at each bus should be discretized at fixed steps depending on their available unit capacities.

3.2.6. Restrictions on DGRs' outputs

$$0\le P_{s,t,i}^{MT}\le S_{MT,i}^{rated} \quad \forall s,t, \quad \forall i\in\Omega_{MT} \tag{27}$$

$$-N_i^{PV}\cdot Q_{PV,lim}^{unit}\le Q_{s,t,i}^{PV}\le N_i^{PV}\cdot Q_{PV,lim}^{unit} \quad \forall s,t, \quad \forall i\in\Omega_{PV} \tag{28}$$

where $Q_{PV,lim}^{unit}$ is a parameter relevant with solar irradiance, and its numerical value under each time segment can be calculated according to (2).

3.2.7. EVs' participation in V2G activities

$$0\le B_{s,i,k,t}^{cha}\le 1 \quad \forall s,k \quad \forall i\in\Omega_N, \quad \forall t\in\left\{t\middle|T_{i,k}^{ar}<t\le T_{i,k}^{ar}+T_{i,k}^{park}\right\} \tag{29}$$

$$0\le B_{s,i,k,t}^{dis}\le b \quad \forall s,k \quad \forall i\in\Omega_N, \quad \forall t\in\left\{t\middle|T_{i,k}^{ar}<t\le T_{i,k}^{ar}+T_{i,k}^{park}\right\} \tag{30}$$

where $B_{s,i,k,t}^{cha}$ and $B_{s,i,k,t}^{dis}$ are binary variables that respectively indicate the charging and discharging states of $EV_{s,i,k}$ at time segment t. Taking variable $B_{s,i,k,t}^{cha}$ as examples, $B_{s,i,k,t}^{cha}=1$ indicates $EV_{s,i,k}$ is charging at time segment t, while $B_{s,i,k,t}^{cha}=0$ means not. The numerical value of parameter b is assigned according to V2G environments. To be specific, for unidirectional V2G environment, parameter b is valued 0 to avoid EVs' participation in discharging behaviors. While for bidirectional V2G environment, parameter b is valued 1.

3.2.8. Mutual exclusivity of EVs' charging and discharging states

$$0\le B_{s,i,k,t}^{cha}+B_{s,i,k,t}^{dis}\le 1 \quad \forall s,k \quad \forall i\in\Omega_N, \quad \forall t\in\left\{t\middle|T_{i,k}^{ar}<t\le T_{i,k}^{ar}+T_{i,k}^{park}\right\} \tag{31}$$

It is impossible that the charging and discharging activities of a particular EV occur at the same time. This mutual exclusivity is neatly represented in (31).

3.2.9. Power demands of EVCSs

$$P_{s,t,j}^{EV}=P_{EV}^{rated}\cdot\left(\sum_{i\in\Omega_j^{bus}}\sum_{k\in\Omega_{s,i,t}^{EV}}\left(B_{s,i,k,t}^{cha}-B_{s,i,k,t}^{dis}\right)\right) \quad \forall s,t, \quad \forall j\in\Omega_{CF} \tag{32}$$

In this paper, EV owners are assumed to carry out their charging/discharging behaviors at nearest EVCSs, which can be realized by designating EVCS service regions according to Voronoi diagrams [27]. To make the description clear, the set Ω_j^{bus} is defined to represent buses included in the service region of EVCS installed at bus j. Moreover, EVs that head for bus i in season s, and meanwhile are under parking state at time segment t are expressed by $\Omega_{s,i,t}^{EV}$.

3.2.10. Charging satisfaction of EV owners

$$B_{s,i,k,t}^{cha}=1 \quad \forall s, \quad \forall i\in\Omega_N, \quad \forall k\in\left\{k\middle|EV_{s,i,k}\in\Omega_{nd}\right\} \quad \forall t\in\left\{t\middle|T_{i,k}^{ar}<t\le T_{i,k}^{ar}+T_{i,k}^{park}\right\} \tag{33}$$

$$\sum_{t=T_{i,k}^{ar}}^{T_{i,k}^{ar}+T_{i,k}^{park}}\left(B_{s,i,k,t}^{cha}-B_{s,i,k,t}^{dis}\right)=Ceil\left(E_{s,i,k}\middle/\left(P_{EV}^{rated}\cdot\Delta t\right)\right) \quad \forall s, \quad \forall i\in\Omega_N, \quad \forall k\in\left\{k\middle|EV_{s,i,k}\in\Omega_d\right\} \tag{34}$$

where *Ceil* is the ceiling function. To relieve the "range anxieties" of EVs [28], EV owners tend to make their batteries as full as possible when departing EVCSs. For EVs that are impossible to be fully charged due to short park duration (i.e. non-dispatchable EVs), they should be charged at rated power as soon as they enter the parking lots, until departures. While for dispatchable EVs, despite of their participation in V2G activities, they should be equipped with fully charged batteries at their departures.

3.2.11. Restrictions on SOCs of EVs

$$\sum_{t=T_{i,k}^{ar}}^{T}\left(B_{s,i,k,t}^{cha}-B_{s,i,k,t}^{dis}\right)\le Ceil\left(E_{s,i,k}\middle/\left(P_{EV}^{rated}\cdot\Delta t\right)\right), \quad \forall T=T_{i,k}^{ar}+1,T_{i,k}^{ar}+2,\cdots,T_{i,k}^{ar}+T_{i,k}^{park} \quad \forall s, \forall i\in\Omega_N, \forall k\in\left\{k\middle|EV_{s,i,k}\in\Omega_d\right\} \tag{35}$$

$$\sum_{t=T_{i,k}^{ar}}^{T}\left(B_{s,i,k,t}^{cha}-B_{s,i,k,t}^{dis}\right)\geq -1\cdot Floor\left(\left(Cap_{s,i,k}-E_{s,i,k}\right)\Big/\left(P_{EV}^{rated}\cdot\Delta t\right)\right),\quad \forall s,\quad \forall i\in\Omega_N,\quad \forall k\in\{k|EV_{s,i,k}\in\Omega_d$$

where *Floor* is the floor function. It is obvious that EVs with already full batteries are not able to participate in charging behaviors. And similarly, EVs with empty batteries are not applicable for discharging behaviors. That is to say, SOC of each EV should be included in the interval [0, 1] at any time segment. These restrictions are represented in (35) and (36), from the aspects of upper bounds and lower bounds of SOCs, respectively.

3.2.12. Quantities of occupied CFs

$$N_{CF,s,t,j}=\sum_{i\in\Omega_j^{bus}}\sum_{k\in\Omega_{s,i,t}^{EV}}\left(B_{s,i,k,t}^{cha}+B_{s,i,k,t}^{dis}\right)\quad \forall s,t,\quad \forall j\in\Omega_{CF} \tag{37}$$

Based on the novel topology of cables in EVCSs [29], the connection object of a particular CF is regarded to be alterable among various EVs through timely reconfiguration. Thereby, at a certain time segment, EVs that are implementing charging and discharging activities should occupy corresponding CFs in EVCSs. While for inactive EVs (i.e. EVs without power exchange with distribution systems), CFs are not essential.

3.2.13. Sufficiency of CFs in EVCSs

$$N_j^{CF}\geq N_{CF,s,t,j}\quad \forall s,t,\quad \forall j\in\Omega_{CF} \tag{38}$$

In any EVCS, the quantity of installed CFs should be greater than that of occupied CFs at any time segment, as expressed in (38).

3.3. Second order conic relaxation

To process the quadratic constraints expressed in (23), an exact second order conic relaxation is proposed and adopted in this paper. And in consequence, the coordinated allocation model is transformed into the type of MISOCP, whose standard form is comprehensively described in Ref. [21].

The specific steps of relaxation and transformation are shown as follows.

Step 1: Replace the equality sign in (23) with greater than or equal to sign, as shown in (39). This operation is an equivalent one and does not impact the optimal solutions of allocation model.para

$$I_{s,t,ij}^{sqr}\geq\frac{P_{s,t,ij}^2+Q_{s,t,ij}^2}{U_{sub}^2}\quad \forall s,t,\quad \forall ij\in\Omega_L \tag{39}$$

The equivalence of the adopted replacement can be sufficiently proved by using reduction to absurdity. Denote the right part of (39) as $I_{s,t,ij}^{sqr\_base}$ for the purpose of concision, and then the specific proof is described as follows:

Assume that the optimal solution of the proposed allocation model is found at $I_{s,t,ij}^{sqr}=I^{\#}$ and $I^{\#}>I_{s,t,ij}^{sqr\_base}$. Then there must exists a constant $\xi\in[Isqr\_base\ s,t,ij, I^{\#})$ that corresponds to a better solution, since the objective function of optimization model is a monotone increasing function of $I_{s,t,ij}^{sqr}$. The existence of ξ conflicts with the aforementioned assumption, and thus demonstrates that the optimal solution is found at $I_{s,t,ij}^{sqr}=I_{s,t,ij}^{sqr\_base}$. Thereby, the equivalence of the adopted replacement in (39) is effectively proved.

$$\forall T=T_{i,k}^{ar}+1,\ T_{i,k}^{ar}+2,\ \cdots,\ T_{i,k}^{ar}+T_{i,k}^{park} \tag{36}$$

Step 2: With the help of auxiliary variable *Au*, transform (39) to be second order conic constraints and linear constraints, whose formulations are represented in (40) and (41).

$$\left\|\begin{matrix}2P_{s,t,ij}/U_{sub}\\2Q_{s,t,ij}/U_{sub}\\I_{s,t,ij}^{sqr}-Au\end{matrix}\right\|_2\leq I_{s,t,ij}^{sqr}+Au\quad \forall s,t,\quad \forall ij\in\Omega_L \tag{40}$$

$$Au=1 \tag{41}$$

Finally, the relaxed optimization model consists of linear objective function, linear constraints and second order conic constraints, which properly accords with the standard form of MISOCP. The inclusions of the relaxed optimization model are specifically shown in (42).

$$\begin{matrix}\min & (6)\\ s.t. & (17)-(22)(24)-(38)(40)(41)\end{matrix} \tag{42}$$

4. Case study

In this section, a practical urban area fed by a 31-bus distribution system in China is used to test the proposed model and approach. The MISOCP model coded in MATLAB environment is solved by

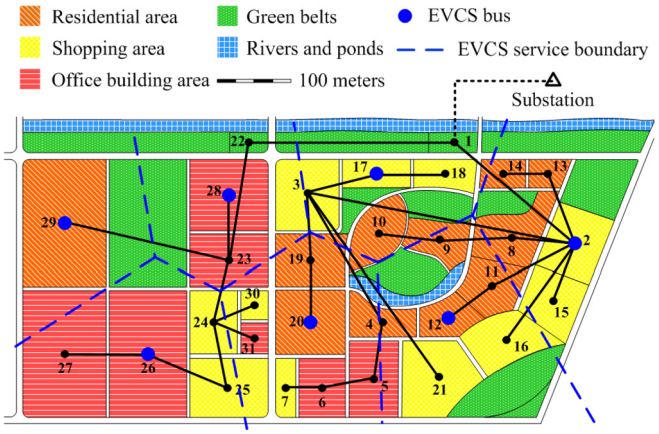

Fig. 3. The practical urban area under study [22].

commercial solver GUROBI through YALMIP platform [30]. And finally, the numerical results are detailedly presented and carefully analyzed, which demonstrate the value of this paper in an effective way.

4.1. Case overview and parameter settings

As shown in Fig. 3, the test system used in this paper is a coupled one with both geographical and electrical information, which are collected from a practical urban area in Jiangsu, China [22]. The land blocks are classified into diverse typical types according to land usages (e.g. residential area, shopping area and office building area), and are marked by different colors. While the electrical part of test system is a 10-kV radial distribution system and its specific parameters can be found in Ref. [22]. As a reasonable simplification, load types are designated to electrical buses, which are consistent with the corresponding usages of land blocks.

With consideration of realistic information, electrical bus sets {2, 3, 6, 20, 21, 23, 25, 29} and {5, 7, 16, 17, 24, 28} are respectively selected as the candidate sites of PV and MT installation. While EVCSs are deployed at electrical buses numbered 2, 12, 17, 20, 26, 28, 29. For the purpose of convenience, electrical buses, EVCSs, as well as EV destinations are supposed to be located at geometrical centers of the land blocks, which make the corresponding distance measurements easy to be achieved. According to the distance data among land blocks, service regions of EVCSs are determined by Voronoi diagrams [27], and in consequence, EVs are designated to their nearest EVCSs to implement charging/discharging behaviors.

Parameters adopted in this study are specified as follows.

1) The employed distribution curves of solar irradiance are minutely described in Fig. 1, which are derived from public data [18]. And the annual peak solar irradiance in this paper is set as 1000 W/m^2.
2) Distribution curves of EVs' arrival numbers and parking durations corresponding to various land usages, as well as the profiles of electrical loads for various scenarios are collected from Ref. [22]. These distribution curves are attached in Appendix A and B, for the direct perception of readers. Moreover, the peak parking number of each land block is estimated according to the corresponding annual peak load, and is revealed in Appendix C.
3) Parameters of DGRs in this paper are derived from Ref. [21], as detailedly shown in Table 1.
4) Parameters of CFs are provided in Table 2. In fact, two kinds of CFs are considered in this paper (i.e. unidirectional CFs and bidirectional CFs). Parameters of unidirectional CFs are derived from the CF with model number NCCP-DC500-030K-GB01, which is produced by Nancal Energy-Saving Technology Co., Ltd [31]. While for bidirectional CFs, owing to the lack of large-scale commercial applications, their parameters are reasonably inferred according to the included components. To be specific, investment cost, as well as O&M cost of bidirectional CFs are assumed to be 20% greater than those of unidirectional CFs, due to the extra costs for bidirectional converters, metering issues, and interface concerns [32]. For the purpose of concision, this growth rate is denoted as r in this paper.
5) The discount rate used in annualization is set to be 0.03 [21].
6) The battery capacity of EV is valued 100 kWh [22].
7) Per-unit cost of purchasing electricity from upper grid is set to be 0.07 $/kWh [33], while per-unit cost of network losses is specified as 0.08 $/kWh [21].
8) Per-unit cost of electricity losses in charging/discharging behaviors is valued 0.08 $/kWh. And the power loss rate in charging/discharging behaviors is set to be 10%.
9) Per-unit cost of EV battery degradation is supposed to be 0.03 $/kWh, which is estimated according to the price of unit battery and battery lifetime cycles [24].
10) The lower and upper limits of voltage magnitudes are respectively set as 0.95 p.u. and 1.05 p.u. in this paper. While for branch current, the permitted maximum branch current is specified to be 400 A.

Table 1
Parameters of DGRs [21].

	PV	MT
Economic life	25 years	10 years
Investment cost	1200 $/kVA	750 $/kVA
O&M cost	2 $/MWh	10 $/MWh
Fuel cost	N/A	120 $/MWh
CO_2 emission	N/A	720 g/kWh
CO_2 emission tax	N/A	10 $/t
Unit capacity in installation	10kVA	10kVA

4.2. Numerical results

For comparison purpose, three cases have been carried out in this subsection. These three cases are with the same system parameters, except for EVs' charging modes. In Case 1, the V2G functions of EVs are neglected (i.e. uncoordinated charging mode). That is to say, EVs under Case 1 are getting charged immediately after arrival and disconnected from CFs as soon as their batteries are fully charged. While in Case 2 and Case 3, the unidirectional V2G and bidirectional V2G functions are respectively considered. Optimal solutions corresponding to different cases are provided in Table 3, and the comparisons from perspectives of allocation schemes and economic costs are shown in Fig. 4 and Fig. 5.

As observed in Fig. 4, the total installation capacities of PV power generation in Case 1, Case 2 and Case 3 are respectively 12.57 MVA, 13.39 MVA and 13.58 MVA, showing an ascendant trend. While in contrast, a reverse trend emerges in the installation of MTs, with the total capacities decreasing from 2.59 MVA to 1.46 MVA, and finally falling to 60 kVA. Moreover, 63 suits of CFs are installed in Case 2, which is significantly less than the 107 suits in Case 1 and 88 suits in Case 3. The aforementioned differences among various optimal allocation schemes essentially derive from the diverse scenario settings corresponding to Cases, and are further explained in the following description. As the DGR with excellent economic performance, the installation of PV power generation can effectively reduce the concerned annualized social cost. However, due to the intermittence of solar irradiance, the non-dispatchable PV active power outputs are not temporally synchronized with the power consumption in distribution systems. The redundant PV power back-feeding to upper power grid would challenge the strength of distribution systems, and thus create restrictions on the maximum capacity of PV installation. In Case 2 and Case 3, the V2G functions make EV power demands temporally dispatchable and in consequence relieve the gap between power generation and consumption at the peak time of PV outputs. Thereby, the installation capacities of PV power generation in Case 2 and Case 3 are greater than that of Case 1. And moreover, Case 3 has the largest installation capacity of PV power generation, since bidirectional V2G function is more flexible than unidirectional V2G function in the adjustment of EV power demands. With regard to MTs, they are dispatchable DGRs with fast response characteristic and always employed to feed local power consumers at peak load time. The employment of MTs can effectively relieve the excessively high load rate of

Table 2
Parameters of CFs.

	Unidirectional CF [22]	Bidirectional CF
Rated power for charging/discharging	30 kW	30 kW
Economic life	10 years	10 years
Investment cost	3250 $/unit	3900 $/unit
O&M cost	325 $/unit/year	390 $/unit/year

Table 3
Optimal solutions of the coordinated allocation models under different cases.

Installation site (bus number)	Case 1 (uncoordinated charging)			Case 2 (unidirectional V2G)			Case 3 (bidirectional V2G)		
	PV capacity (kVA)	MT capacity (kVA)	CF quantity (suit)	PV capacity (kVA)	MT capacity (kVA)	CF quantity (suit)	PV capacity (kVA)	MT capacity (kVA)	CF quantity (suit)
2	4720	–	23	5530	–	11	2030	–	21
3	1140	–	–	690	–	–	1180	–	–
5	–	550	–	–	330	–	–	40	–
6	480	–	–	740	–	–	480	–	–
7	–	180	–	–	70	–	–	–	–
12	–	–	26	–	–	17	–	–	26
16	–	150	–	–	–	–	–	–	–
17	–	1710	17	–	1060	11	–	20	13
20	540	–	16	560	–	9	3930	–	13
21	690	–	–	620	–	–	710	–	–
23	4390	–	–	4540	–	–	4760	–	–
25	450	–	–	540	–	–	430	–	–
26	–	–	8	–	–	5	–	–	5
28	–	–	12	–	–	7	–	–	7
29	160	–	5	170	–	3	60	–	3
Total installation	12570	2590	107	13390	1460	63	13580	60	88
C^I ($\times 10^6$ $)	1.1347			1.0751			0.9814		
$C^{O\&M}$ ($\times 10^4$ $)	9.9184			8.1254			9.1477		
$C^{F\&E}$ ($\times 10^5$ $)	1.4839			0.5845			0.0225		
C^P ($\times 10^5$ $)	1.8244			1.1151			1.1453		
C^{NL} ($\times 10^3$ $)	1.1929			1.2541			1.9992		
C^{CL} ($\times 10^4$ $)	4.3421			4.3421			5.1447		
C^B ($\times 10^5$ $)	1.6283			1.6283			1.9293		
Annualized social cost ($\times 10^6$ $)	1.7722			1.5338			1.4360		

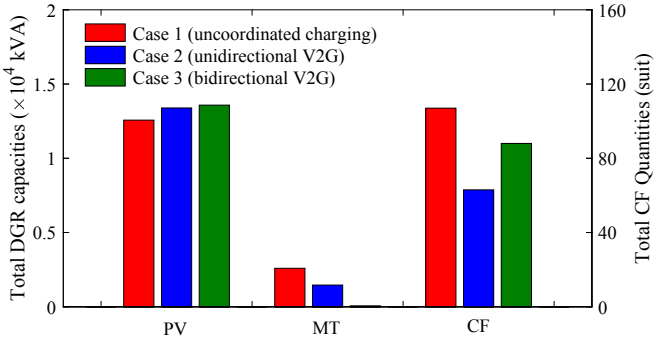

Fig. 4. Comparison on total installation capacities/quantities of DGRs and CFs.

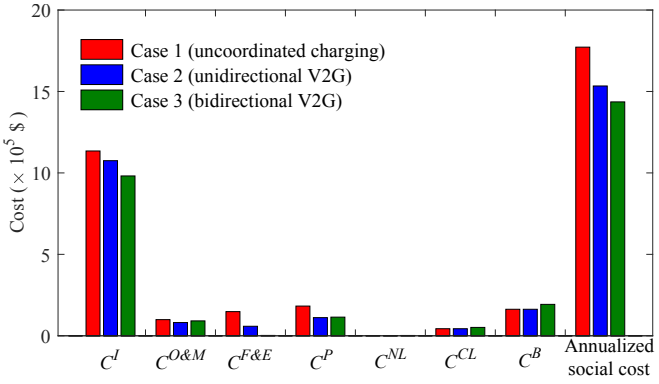

Fig. 5. Comparison on cost items.

upstream electrical feeders and reduce network losses. The only weakness of MT is the expensive unit investment cost and fuel cost, which tends to increase the corresponding annualized social cost. In Case 1, due to the limited feeder capacity, a large number of MTs are compelled to be allocated to deal with the heavy load scenario. While under V2G environments, the occurrence frequency of heavy load scenario apparently decreases, owing to the temporally dispatchable characteristic of EV power demands. Especially in Case 3, EVs under bidirectional V2G environment can act as power sources when necessary, which make the total installation capacity of MT fall to a very low level (i.e. 60 kVA). Finally, regarding the installation of CFs, it is easy to understand that Case 1 has the largest quantity of CFs, as the uncoordinated charging mode is with the lowest CF utilization rate. While in Case 2 and Case 3, the utilization of CFs is arranged in an optimal way, and in consequence decreases the installation quantity of CFs. Furthermore, Case 2 has the least quantity of CFs, since EVs under bidirectional V2G environment participate in the distribution system operation in a more frequent way and meanwhile occupy CFs for longer time.

On the basis of Fig. 5, it is easy to find that the differences among various allocation schemes are also reflected in cost items. To be detailed, C^I is the most weighted part of annualized social cost, and

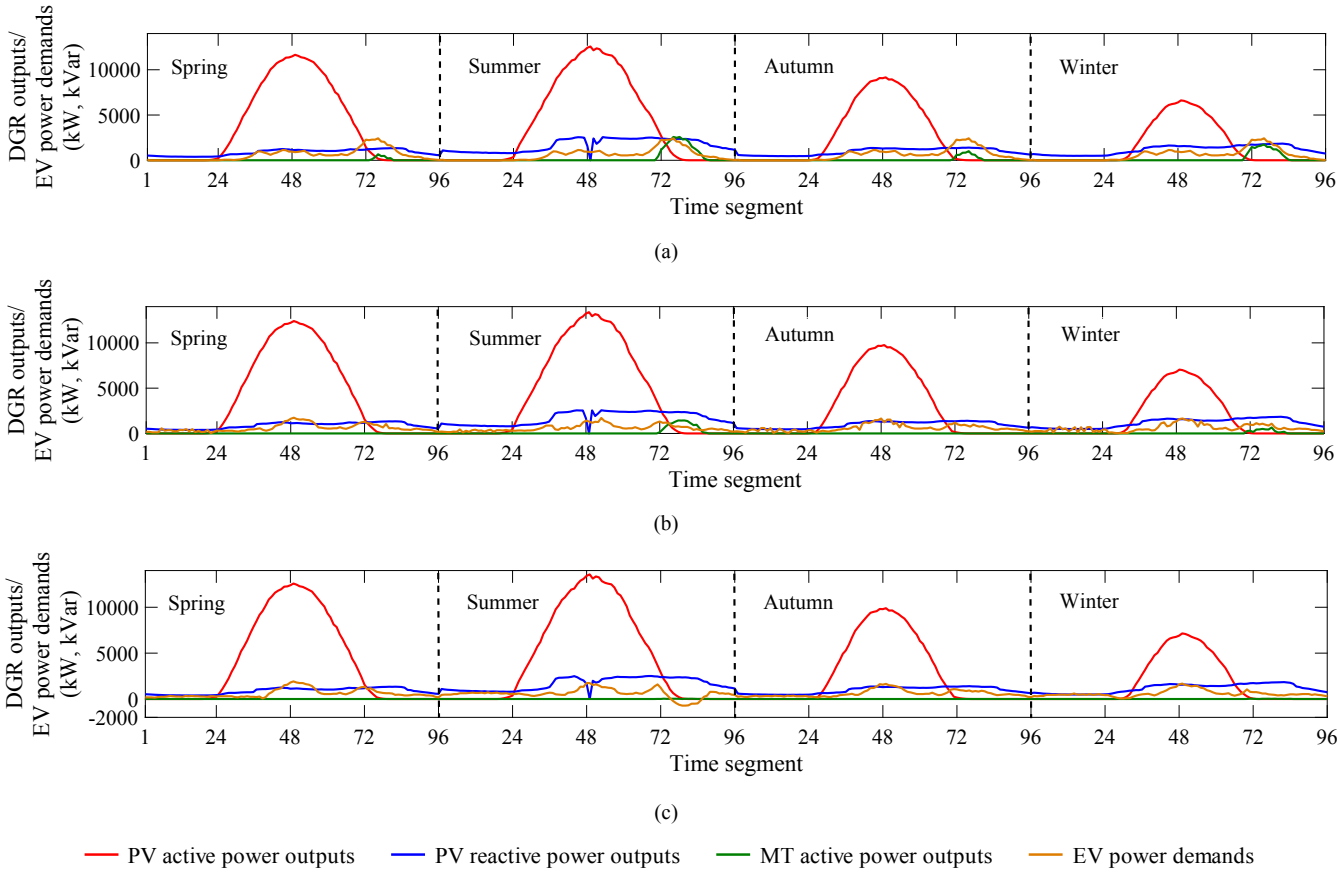

Fig. 6. DGR outputs and EV power demands in workdays under optimal allocation schemes. (a) Case 1 (uncoordinated charging); (b) Case 2 (unidirectional V2G); (c) Case 3 (bidirectional V2G).

shows a downward trend from Case 1 to Case 3. This downward trend is mainly caused by the degressive installation capacities of MTs, similar with that of $C^{F\&E}$. While in $C^{O\&M}$, Case 2 has the smallest numerical value, owing to its least installation quantity of CFs, as well as the cheaper unit O&M cost compared with Case 3. With regard to C^{P}, the DSO of Case 1 purchases the largest number of electricity from upper grid, for the purpose of compensating the deficiency in PV capacity. Subsequently, it is apparent that the numerical values of C^{NL} are quite small, when compared with the other cost items. This phenomenon derives from the short power-supply distance of the test system, which brings about small resistance and reactance. In terms of C^{CL} and C^{B}, both of them are relevant with the charging/discharging electricity of EVs, and thereby their numerical values show the same variation trend. To be specific, numerical values of C^{CL} and C^{B} under Case 3 are slightly greater than those of Case 1 and Case 2, since EVs under bidirectional V2G environment exchange more electricity with distribution systems. Finally, viewed in a comprehensive way, Case 3 is the most beneficial option with least annualized social cost, orderly followed by Case 2 and Case 1.

Furthermore, to clearly exhibit the influence of V2G functions on optimal allocation schemes of DGRs and EVCSs, Fig. 6 and Fig. 7 display the actual DGR outputs and EV power demands corresponding to all the time segments under consideration, respectively for workdays and weekends. As observed in Figs. 6 and 7, the peak PV output occurs at 12.15 p.m. in Summer, and the peak net load appears around 8.00 p.m. in Summer. Performances of DGRs and EVs under these two time segments would largely impact the corresponding allocation schemes. In Case 1, EV charging demands are temporally non-dispatchable, and thereby the only effective option of DSOs is to increase MT active power outputs around peak net load time, which helps to avoid branch current violation in upstream electrical feeders. While in Case 2 and Case 3, some of the EVs arriving at morning are scheduled to be charged at peak PV output time, so as to consume the redundant PV power. And meanwhile, the original EV charging demands at peak net load time are transferred to late night, which distinctly reduces DSOs' dependence on MTs. It is notable that EVs under Case 3 feed impressive electricity into the distribution system at peak net load time, and consequently the effects of MTs almost disappear.

In summary, the aforementioned comparison and analysis based on numerical results convincingly demonstrate the positive effects of EVs' V2G functions. To be specific, the temporally dispatchable characteristic of EV power demands under V2G environments makes the distribution system operate in a flexible way. This phenomenon effectively improves the permitted capacity of PV integration, and simultaneously relieves DSOs' dependence on expensive MTs. Consequently, the allocation schemes of DGRs and EVCSs are significantly refined, and load demands in the target area are satisfied with lower annualized social costs. In addition, the allocation scheme under bidirectional V2G environment is more economical than that under unidirectional V2G environment, as EV power demands have greater degrees of adjustment margins.

4.3. Exactness of the second order conic relaxation

To numerically demonstrate the exactness of the second order conic relaxation, deviation variables are introduced in this

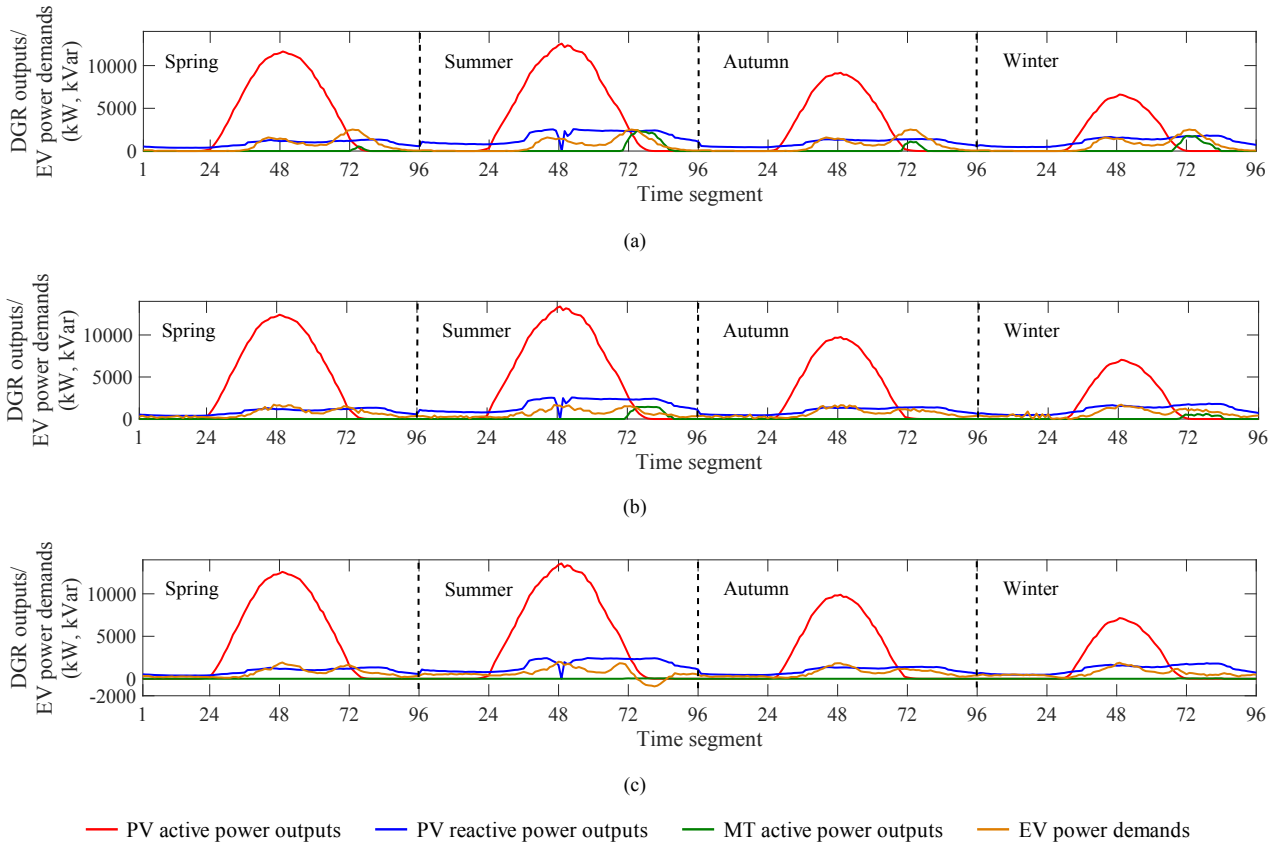

Fig. 7. DGR outputs and EV power demands in weekends under optimal allocation schemes. (a) Case 1 (uncoordinated charging); (b) Case 2 (unidirectional V2G); (c) Case 3 (bidirectional V2G).

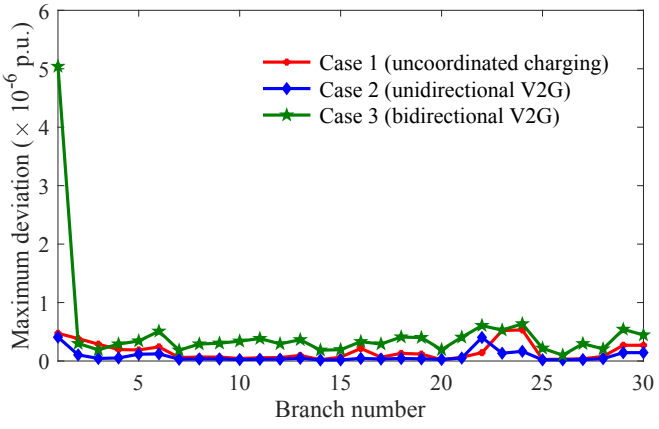

Fig. 8. Maximum values of deviation variables at different branches.

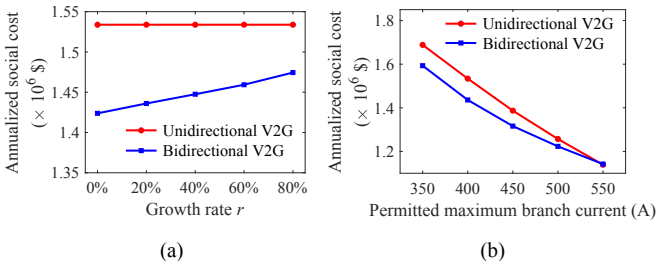

Fig. 9. Sensitivity analysis on parameters. (a) Growth rate r; (b) Permitted maximum branch current.

subsection, as formulated in (43).

$$\Delta_{s,t,ij} = \left| I^{sqr}_{s,t,ij} - \frac{P^2_{s,t,ij} + Q^2_{s,t,ij}}{U^2_{sub}} \right| \quad \forall s,t, \quad \forall ij \in \Omega_L \tag{43}$$

For each branch, the maximum numerical values of deviation variables among all the 768 time segments are shown in Fig. 8. And it is obvious that the deviations of second order conic relaxation in this paper stay in the order of 10^{-6}, which is quite small and should be regarded as the reasonable error in numerical calculations. Therefore, the adopted relaxation in (39) is proved to be an equivalent procedure, and does not impact the accuracy of the proposed model and approach.

4.4. Sensitivity analysis

Benchmarked by the optimal allocation schemes under unidirectional V2G environment, the extra economic benefits derived from modifying unidirectional CFs into bidirectional CFs are impacted by various factors, typically the increased investment and O&M costs of CFs, as well as the strength of distribution systems. In this subsection, the unit investment cost and O&M cost of bidirectional CFs are orderly set to be 0%, 20%, 40%, 60% and 80% more expensive than those of unidirectional CFs, based on which the annualized social costs under bidirectional V2G environment are carefully compared with those under unidirectional V2G environment, as shown in subfigure (a) of Fig. 9. In addition, as an important index of distribution system strength, the permitted maximum branch current is orderly assigned by various values, ranged from 350 A to 550 A. And the corresponding comparison is

shown in subfigure (b) of Fig. 9.

As observed in subfigure (a) of Fig. 9, the annualized social cost under bidirectional V2G environment shows synchronous growth with the unit investment cost and O&M cost of bidirectional CFs. Compared with the constant annualized social cost under unidirectional V2G environment, the extra economic benefits derived from modifying unidirectional CFs into bidirectional CFs are considerably reduced. The authors can even reasonably infer that the allocation schemes considering unidirectional V2G functions would be more economical when bidirectional CFs are far more expensive than unidirectional CFs. Therefore, as the charging mode being not yet under large-scale commercial applications, prospects of bidirectional utilization of EVs, as well as the economic benefits of allocation schemes under bidirectional V2G environment, are largely impacted by the price of bidirectional CFs.

While in subfigure (b) of Fig. 9, the presented comparison reveals that the stronger the distribution system, the less economic advantage allocation schemes under bidirectional V2G environment will have. When the permitted maximum branch current of the test system is set to be 550 A or even greater value, the allocation scheme under unidirectional V2G environment is more economical than that under bidirectional V2G environment. This phenomenon is reasonable and can be explained in a proper way. To be detailed, the installation capacities of expensive MTs would be sharply reduced in strong distribution systems, since DSOs can purchase much more electricity from upper grids with lower costs than MT power generation. And meanwhile, the reduced network losses costs owing to EVs' V2G behaviors are distinctly less than the corresponding wastes on charging/discharging losses and battery degradation of EVs. In consequence, cost-effectiveness of the utilization of EVs' V2G functions drastically declines in strong distribution systems, and the extra investment and O&M costs make allocation schemes under bidirectional V2G environment more disadvantaged.

5. Conclusion

This paper proposes an optimization model for the coordinated allocation of DGRs and EVCSs, during which the V2G functions of EVs are comprehensively considered. With the utilization of linearized Distflow equations, as well as second order conic relaxation, the optimization model is formulated as a MISOCP problem, which is ideally convex and can be effectively solved by off-the-shelf commercial solvers. A coupled geographical-electrical system derived from practical urban areas is employed as the test system in this paper, and the main conclusions are summarized as follows.

1) With consideration of EVs' V2G functions, the optimal sites and sizes of DGRs, as well as the optimal sizes of EVCSs can be properly determined by the proposed model and approach.
2) Compared with uncoordinated charging modes, utilization of EVs' V2G functions effectively improves the permitted capacity of PV integration, and simultaneously relieves DSOs' dependence on expensive MTs, which makes the allocation schemes of DGRs and EVCSs more economical.
3) Although allocation schemes under bidirectional V2G environment are more economical than those under unidirectional V2G environment in most circumstances, prospects of EVs' bidirectional utilization are challenged by the expensive investment and O&M costs of bidirectional CFs, as well as the strength of future distribution systems.

Acknowledgment

This work was financially supported by the Project of Jiangsu Key Laboratory of Smart Grid Technology and Equipment, the National Natural Science Foundation of China (No. 51707033) and the Scientific Project of Jiangsu Electric Power Company (No. J2018003).

Appendix

A. Typical distributions of electric vehicles' arrival numbers and parking durations

Fig. 10 and 11 show the typical distribution curves of EVs' arrival numbers and parking durations collected from Ref. [22].

B. Typical load profiles

Fig.12 illustrates the typical load profiles collected from Ref. [22].

C. Electric vehicles' peak parking number of each land block

For each land block, EVs' peak parking number is provided in Table 4.

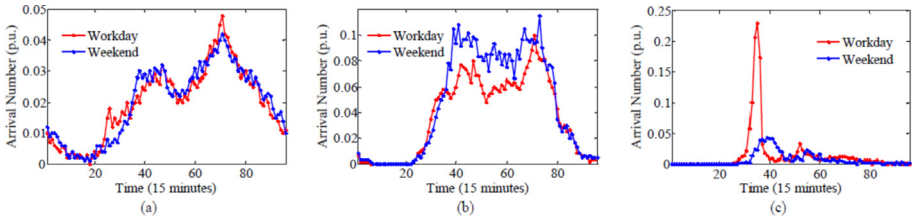

Fig. 10. Typical distribution of EVs' arrival numbers. (a) residential area; (b) shopping area; (c) office building area [22].

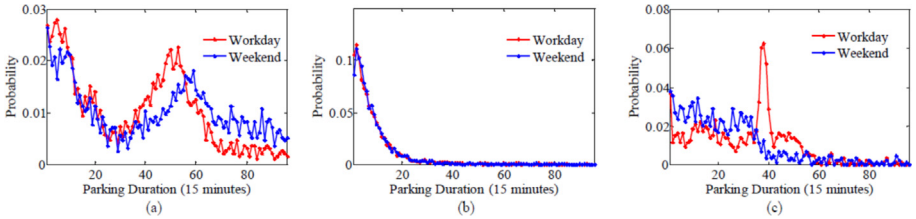

Fig. 11. Typical distribution of EVs' parking durations. (a) residential area; (b) shopping area; (c) office building area [22].

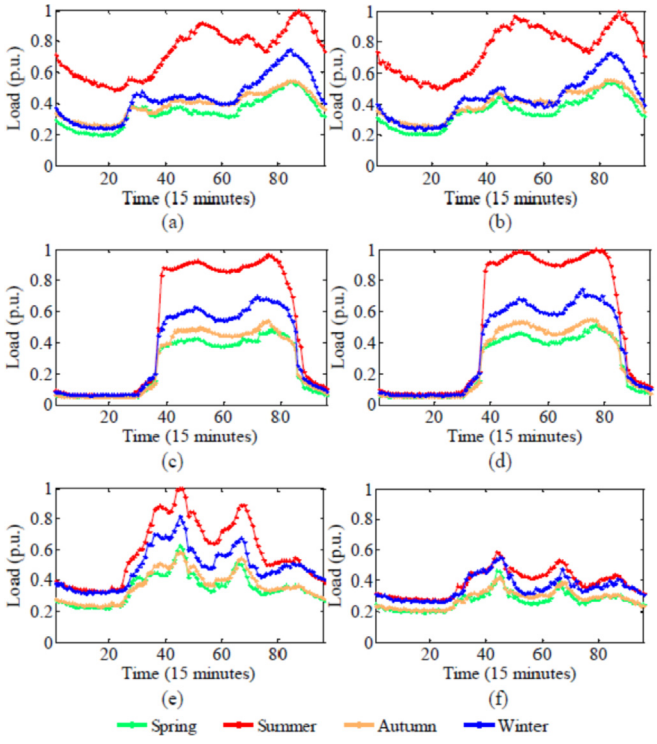

Fig. 12. Typical load profiles of different scenarios. (a) workdays in residential areas; (b) weekends in residential areas; (c) workdays in shopping areas; (d) weekends in shopping areas; (e) workdays in office building areas; (f) weekends in office building areas [22].

Table 4
EVs' Peak Parking Number of Each Land Block

Block number	EVs' peak parking number	Block number	EVs' peak parking number
1	0	17	6
2	10	18	6
3	4	19	6
4	5	20	6
5	4	21	16
6	4	22	0
7	2	23	2
8	5	24	4
9	5	25	2
10	5	26	1
11	5	27	1
12	5	28	10
13	3	29	4
14	3	30	2
15	8	31	1
16	6		

References

[1] Mehigan L, Deane JP, Gallachóir BPÓ, Bertsch V. A review of the role of distributed generation (DG) in future electricity systems. Energy 2018;163:822–36.
[2] Guille C, Gross G. A conceptual framework for the vehicle-to-grid (V2G) implementation. Energy Policy 2009;37(11):4379–90.
[3] Aghajani S, Kalantar M. Optimal scheduling of distributed energy resources in smart grids: a complementarity approach. Energy 2017;141:2135–44.
[4] Mahdavi S, Hemmati R, Jirdehi MA. Two-level planning for coordination of energy storage systems and wind-solar-diesel units in active distribution networks. Energy 2018;151:954–65.
[5] Davidov S, Pantoš M. Optimization model for charging infrastructure planning with electric power system reliability check. Energy 2019;166:886–94.
[6] Amini MH, Moghaddam MP, Karabasoglu O. Simultaneous allocation of electric vehicles' parking lots and distributed renewable resources in smart power distribution networks. Sustain Cities Soc 2017;28:332–42.
[7] Zhang H, Moura S, Hu Z, Qi W, Song Y. Joint PEV charging station and distributed PV generation planning. IEEE Power and Energy Soc Gen Meet 2017.
[8] Zhang H, Moura SJ, Hu Z, Qi W, Song Y. Joint PEV charging network and distributed PV generation planning based on accelerated Generalized Benders Decomposition. IEEE Trans Transp Electrif 2018;4(3):789–803.
[9] Kandil SM, Farag HEZ, Shaaban MF, El-Sharafy MZ. A combined resource allocation framework for PEVs charging stations, renewable energy resources and distributed energy storage systems. Energy 2018;143:961–72.
[10] Sortomme E, El-Sharkawi MA. Optimal charging strategies for unidirectional vehicle-to-grid. IEEE Trans Smart Grid 2011;2(1):131–8.
[11] Gao S, Chau KT, Liu C, Wu D, Chan CC. Integrated energy management of plug-in electric vehicles in power grid with renewables. IEEE Trans Veh Technol 2014;63(7):3019–27.
[12] Morais H, Sousa T, Vale Z, Faria P. Evaluation of the electric vehicle impact in the power demand curve in a smart grid environment. Energy Convers Manag 2014;82:268–82.
[13] Jian L, Zhu X, Shao Z, Niu S, Chan CC. A scenario of vehicle-to-grid implementation and its double-layer optimal charging strategy for minimizing load variance within regional smart grids. Energy Convers Manag 2014;78:508–17.
[14] Sortomme E, El-Sharkawi MA. Optimal scheduling of vehicle-to-grid energy and ancillary services. IEEE Trans Smart Grid 2012;3(1):351–9.
[15] Wang L, Sharkh S, Chipperfield A. Optimal coordination of vehicle-to-grid batteries and renewable generators in a distribution system. Energy 2016;113:1250–64.
[16] Mao T, Lau W, Shum C, Chung HS, Tsang K, Tse NC. A regulation policy of EV discharging price for demand scheduling. IEEE Trans Power Syst 2018;33(2):1275–88.
[17] Faddel S, Aldeek A, Al-Awami AT, Sortomme E, Al-Hamouz Z. Ancillary services bidding for uncertain bidirectional V2G using fuzzy linear programming. Energy 2018;160:986–95.
[18] UO solar radiation monitoring laboratory. Available: http://solardat.uoregon.edu/download/MthAvg/MOMAQ12.txt.
[19] Liu Z, Wen F, Ledwich G. Optimal siting and sizing of distributed generators in distribution systems considering uncertainties. IEEE Trans Power Deliv 2011;26(4):2541–51.
[20] Varma RK, Rahman SA, Vanderheide T. New control of PV solar farm as STATCOM (PV-STATCOM) for increasing grid power transmission limits during night and day. IEEE Trans Power Deliv 2015;30(2):755–63.
[21] Luo L, Gu W, Zhang X, Cao G, Wang W, Zhu G, You D, Wu Z. Optimal siting and sizing of distributed generation in distribution systems with PV solar farm utilized as STATCOM (PV-STATCOM). Appl Energy 2018;210:1092–100.
[22] Luo L, Gu W, Zhou S, Huang H, Gao S, Han J, Wu Z, Dou X. Optimal planning of electric vehicle charging stations comprising multi-types of charging facilities. Appl Energy 2018;226:1087–99.
[23] Fazelpour F, Vafaeipour M, Rahbari O, Rosen MA. Intelligent optimization to integrate a plug-in hybrid electric vehicle smart parking lot with renewable energy resources and enhance grid characteristics. Energy Convers Manag 2014;77:250–61.
[24] Zhao Y, Noori M, Tatari O. Vehicle to Grid regulation services of electric delivery trucks: economic and environmental benefit analysis. Appl Energy 2016;170:161–75.

[25] Shahidehpour M, Wang X, Jiang C, Li Z. Coordinated planning strategy for electric vehicle charging stations and coupled traffic-electric network. IEEE Trans Power Syst 2019;34(1):268–79.
[26] Yeh HG, Gayme DF, Low SH. Adaptive VAR control for distribution circuits with photovoltaic generators. IEEE Trans Power Syst 2012;27(3):1656–63.
[27] Zhang H, Hu Z, Xu Z, Song Y. An integrated planning framework for different types of PEV charging facilities in urban area. IEEE Trans Smart Grid 2016;7(5):2273–84.
[28] Dong J, Liu C, Lin Z. Charging infrastructure planning for promoting battery electric vehicles: an activity-based approach using multiday travel data. Transp Res Part C 2014;38:44–55.
[29] Zhang H, Hu Z, Xu Z, Song Y. Optimal planning of PEV charging station with single output multiple cables charging spots. IEEE Trans Smart Grid 2017;8(5):2119–28.
[30] Qiu H, Zhao B, Gu W, Bo R. Bi-level two-stage robust optimal scheduling for AC/DC hybrid multi-microgrids. IEEE Trans Smart Grid 2018;9(5):5455–66.
[31] Nancal Energy-Saving Technology Co., Ltd. Available: http://www.nancal.com/english/.
[32] Yilmaz M, Krein PT. Review of the impact of vehicle-to-grid technologies on distribution systems and utility interfaces. IEEE Trans Power Electron 2013;28(12):5673–89.
[33] Wu Z, Liu Y, Gu W, Zhou J, Li J, Liu P. Decomposition method for coordinated planning of distributed generation and distribution network. IET Gener, Transm Distrib 2018;12(20):4482–91.